RSC Advances

PAPER

View Article Online
View Journal | View Issue

Cite this: *RSC Adv.*, 2025, **15**, 20446

Facile synthesis of hierarchical structured TiO_2 spheres for high-efficiency mesostructured perovskite solar cells†

Khalid Mahmood, *[a] Usama[a] and Arshi Khalid*[b]

Received 10th February 2025
Accepted 3rd June 2025

DOI: 10.1039/d5ra00966a

rsc.li/rsc-advances

The formation of an electron transport layer (ETL) in perovskite solar cells (PSCs) plays a significant role in their performance and long-term stability. Researchers have focused on exploring suitable ETL materials with large surface areas and proper nanostructures for developing stable and efficient PSCs. The use of TiO_2 spheres as an ETL in PSCs will help to improve high absorber loading and carrier transport. Herein, the growth of hierarchical structured TiO_2 spheres enhanced device performance and stability owing to better morphology and efficient electron ejection from the absorber layer. Eventually, an averaged maximum power conversion efficiency of 21.3% was attained when 3D hierarchical TiO_2 nanorod-sphere ETLs were employed in PSCs. We believe that our work brings a novel vision for the development and design of highly effective hybrid photovoltaics.

1. Introduction

Perovskite solar cells (PSCs) are the so-called "third generation solar cells" that have recently come into the spotlight and are now being widely promoted as viable alternatives to conventional solar cell technologies in terms of cost and environmental impact, addressing the world's challenges in energy production, and environmental impact.[1,2] As possible substitutes to silicon-based solar cells, perovskite solar cells (PSCs) are contenders for future solar cell technology owing to their low material costs, modest production procedures, and promising performances.[3–5] In a mesostructured PSC, the perovskite absorber layer is deposited over the surface of a mesoporous TiO_2 film, which receives photoexcited electrons from the absorbers and transports them to the fluorine-doped tin oxide (FTO) glass substrate.[6–8] A common mesoscopic film in PSC consists of 20–50 nm-sized nanoparticles. However, the disordered size range of TiO_2 nanoparticles leads to increased charge transport distance and scattering probability of photogenerated electrons, resulting in high carrier transport loss. Hence, it is significant to explore supreme mesoporous materials that possess an ample pore size, prolonged interaction zones, and hole-free nanostructures with insignificant margins to stop charge recombination.[9–11] Smaller-sized TiO_2 nanoparticles (NPs) possess high surface area; however, their small pore size limits the penetration of the perovskite absorber into the electron transport layer (ETL). Meanwhile, bigger-sized TiO_2 NPs have a smaller surface area, which disturbs effective charge inoculation over the hole transport layer (HTL). Consequently, it is vital to grow an improved mesostructured material with comparatively moderate-sized TiO_2 NPs to efficiently collect the electrons from the perovskite film. An ETL composed of TiO_2 spheres produced by various methods may be applied in perovskite devices owing to their greater surface area and ability to prevent carrier recombination at perovskite/TiO_2 interfaces.[12,13] It is difficult to produce such hierarchical structures using multi-step procedures such as hydrolysis, solvothermal methods and sol–gel techniques. Recent studies promote the electrostatic spray (e-spray) approach as an inexpensive and straightforward method for depositing thin layers using colloidal solutions. Modern material technologies, nanotechnology, microelectronics, and TiO_2 electrodes for solar cells can benefit from using this technology to deposit different ceramic and polymer powders.[14–16] The benefit of this technique is that it can create TiO_2 nanoclusters as nanoscale spheres without the need for traditional sol–gel synthesis processes.[17] Electrospraying is used to apply a finely dispersed mixture of readily obtainable nano-sized TiO_2 units in EtOH instead of surfactants and essences on a fluorine-doped tin oxide (FTO) substrate for dye-sensitized solar cell (DSSC) photoelectrodes.[18,19]

Currently, efforts devoted to overcome the struggle between light collection and charge transport are focused on constructing nano-chunks on one-dimensional (1D) trunks (*e.g.*, nanotubes and nanorods), *i.e.*, hierarchical designs with scalable engineering.[20–22] Electron transport is feasible through 1D

[a]*Department of Chemical & Polymer Engineering, University of Engineering & Technology Lahore, Faisalabad Campus, 3-1/2 Km. Khurrianwala - Makkuana By-Pass, Faisalabad, Pakistan*

[b]*Department of Humanities & Basic Sciences, University of Engineering & Technology Lahore, Faisalabad Campus, 3-1/2 Km. Khurrianwala - Makkuana By-Pass, Faisalabad, Pakistan. E-mail: khalid@uet.edu.pk; Arshi.khalid@uet.edu.pk*

† Electronic supplementary information (ESI) available. See DOI: https://doi.org/10.1039/d5ra00966a

trunks, although the surface nanostructures can raise the surface area for perovskite loading.[21,22] However, owing to the insignificant surface area of 1D trunks, partial nano-chunks get constructed on their surface, which confines the surface area of the hierarchical nanostructures for perovskite pore filling and loading. Therefore, we attempted to construct a novel TiO_2 hierarchical assembly containing 3D spheres attached to primary 1D nanorod trunks. Thus far, extensive research works have been done on growing 3D hierarchical nanowire assemblies,[19,23–26] as they have applications in solar cells, energy storage and photocatalysis.[27–30] Investigations have been carried out to grow 3D hierarchical nanorod structures using various methods, namely, pulsed laser deposition, sol–gel method, and hydrothermal method.[31–34] However, the combination of electrospray-deposited TiO_2 spheres with hydrothermally grown TiO_2 nanorod branches has not yet been explored for PSCs. This improved growth procedure allows the formation of novel 3D hierarchical bunchy TiO_2 microspheres, offering the advantages of both 3D architectures and hierarchical constructions.

In this study, we performed an exclusive combination of electrospray and hydrothermal methods for growing 3D hierarchical TiO_2 nanostructures as ETLs for PSCs. The 3D hierarchical TiO_2 nanorod-sphere nanostructure-based ETL with optimal electron transport and carrier lifetime produced extremely efficient mesostructured perovskite devices with an average power conversion efficiency (PCE) of 19.54% and a maximum of 21.3%. This extraordinary performance was attributed to the 3D hierarchical structure of the ETL with optimum electron transportation and better nanostructure formation achieved by the electrospray-hydrothermal combined synthesis route. By providing electrons with a direct route to the ETL through the perovskite layer, the nanorod shape reduced electron recombination and increased the overall effectiveness of charge extraction from the perovskite. Because TiO_2 spheres possessed a large surface area, there were many locations available for deposition of the perovskite absorber layer, which increased light absorption and photocurrent production. Thus, this effort proved the extraordinary returns in using hierarchical ETLs for realizing highly effective, large-area, and cost-effective perovskite devices.

2. Experimental section

2.1. Synthesis of TiO_2 nanospheres

TiO_2 nanospheres were produced *via* electrospray technique.[35,36] An 8% (w/v) P-25 (Degussa) nanocrystalline-TiO_2 powder (75% anatase and 25% rutile) was evenly distributed in anhydrous ethanol using an ultrasonic bath for 30 min. The well mixed solution was then electro-sprayed onto FTO glass substrates. A voltage of 13 kV was used with a precursor flowrate of 35 $\mu L\ min^{-1}$.

2.2. Hydrothermal growth of TiO_2 3D hierarchical structure over the nanosphere surface

The hydrothermal method was used to grow a 3D TiO_2 hierarchical structure over a nanosphere surface.[8] In a distinctive procedure, 20 mL of 37% hydrochloric acid was poured into 20 mL of deionized water and sonicated for 5 min. Then, 0.7 mL of titanium(IV) *n*-butoxide was added and further sonicated for 5 min. FTO glasses coated with electrospun TiO_2 nanospheres were placed as slanted inside a Teflon liner autoclave. The above prepared mixture was placed inside the autoclave with the oven preheated to 160 °C and incubated for 1.5 h to grow the desired TiO_2 nanorods over the nanosphere surface. Then, the autoclave was cooled to ambient conditions. The substrates were washed carefully and heated at 300 °C for 30 min for further use.

2.3. Perovskite device construction

First, a dense film of TiO_2 was formed on top of FTO substrates. Mesoporous layers of TiO_2 nanospheres and 3D hierarchical structure were deposited onto the FTO substrates (coated with TiO_2 compact film) using electrospray as described earlier. Then, a layer of perovskite absorber was formed using a commonly developed two-step technique, as previously described by our group.[37,38] Lead iodide mixture formed in *N*,*N*-dimethylformamide (462 mg mL^{-1}) was spin-coated (at 6500 rpm for 60 s) onto the TiO_2 nanostructures, followed by heating it to 70 °C and subsequent cooling to ambient conditions. After that, they were immersed in a CH_3NH_3I solution formed in 2-propanol (10 mg L^{-1}) for 20 s, rinsed with 2-propanol and finally, dried at 70 °C for 15 min. Further processing was done using toluene (0.2 mL) for whole surface exposure. Then, the substrates were spinned at 7500 rpm for 10 s and heated at 70 °C for 15 min. A solution composed of 72.3 mg spiro-OMETAD as a hole-transporting material (HTM) was spin-coated at 4000 rpm for 30 s. A gold (Au) layer with a thickness of 60 nm was deposited *via* thermal evaporation. The active area of the fabricated devices was 0.25 cm^2.

2.4. Characterizations

The top and side-view scanning electron (SEM) pictures of oxide layers were observed together *via* SEM (JEOL-6701F). X-ray diffraction (XRD) was utilized to verify the crystallinity and estimate the phase of TiO_2 spheres. Brunauer–Emmett–Teller (BET) was utilized to estimate the precise surface area *via* adsorption numbers of isotherms. The pore size distributions were found using the adsorption numbers of isotherms founded on a Barrett–Joyner–Halenda (BJH) model. Current density–voltage (*J*–*V*) assessments were made *via* a Keithley source measurement piece (model 2400) under AM 1.5 G illumination (100 mW cm^{-2}). The external quantum efficiency (EQE) data of the perovskite devices was collected *via* a quantum efficiency measurement structure. The steady-state photoluminescence (PL) spectra were obtained using a FluoroMax-4 spectrofluorometer. The electron lifetime for charge conveyance and recombination was attained using a transient photocurrent-voltage spectroscopy arrangement.

3. Results and discussion

In this study, an innovative and simple electrospray technique was used to deposit TiO_2 sphere ETLs with high surface area

and fast electron transference, as shown in Fig. 1a. The e-spray procedure is recognized to be effective in constructing metal-oxide semiconducting nanoarchitectures in a shorter time. Furthermore, this method can be easily applied in industries owing to its cost-effectiveness and feasible coating technique, making it applicable for enormous areas and effortless commercialization. In Fig. 1c, it was observed that electro-sprayed-deposited nanospheres were monodispersed during the whole fabrication procedure, consisting of P-25 as tiny, aggregated particles. Low vapor pressure of the solvent (ethanol) was mandatory to produce spheres. Additionally, the electrospray-deposited spheres generated a complete sphere rather than a hollow form. This happened owing to the speedy disappearance of solvent, having a comparatively higher vapor pressure on the outside of the small sized droplets of TiO_2. Therefore, intense convection forces helped in the formation of fitted aggregates.[39] These nanospheres exhibited high sponginess, good compactness, and a unique web-like structure that was extremely helpful for the broad penetration of perovskite absorber into it. The functionality of TiO_2 nanosphere-based ETLs was further enhanced by mounting the nanorods over the whole outer surface of TiO_2 nanospheres *via* the hydrothermal method (Fig. 1b). Notably, such a TiO_2 3D hierarchical structure over the nanosphere surface (see SEM image in Fig. 1d) with a unique morphology offered faster charge transport, enhanced perovskite infiltration and a larger surface area.

Magnified SEM images of the ETLs consisting of TiO_2 nanospheres and TiO_2 3D hierarchical structure (growth of nanorods over nanospheres surface) can be clearly seen in Fig. 2a and b, respectively. The electrospraying parameters, such as the solution concentration, precursor flow rate and applied bias, were carefully chosen for the formation of TiO_2 nanospheres formed with small TiO_2 nanoparticles (60–70 nm diameter) and prominent inner porosity within the nanosphere (Fig. 2a). The deposition of a mesoporous nanosphere is also a prerequisite to grow the 3D hierarchical structure through the hydrothermal step. In Fig. 2b, it was obviously observed that nanorods were uniformly grown over the whole outer region of the nanospheres, making it a perfect 3D hierarchical assembly. We expected that the TiO_2 3D hierarchical assembly (Fig. 2b) must have numerous significant paybacks, such as faster electron transport, enhanced surface area and better pore filling compared with TiO_2 nanospheres. As revealed in Table S1,† the surface areas were 70.4 and 90.1 $m^2\ g^{-1}$ for electrospray deposited TiO_2 nanospheres and 3D hierarchical structured TiO_2, respectively. A comparison of 3D hierarchical structured TiO_2 (Fig. 2b) with the TiO_2 sphere ETLs (Fig. 2a) evidently established the variances in pore volume: the pore volume decreased from 1.35 to 0.85 $cm^3\ g^{-1}$, respectively (Table S1†). The TiO_2 nanospheres were formed of typical micropores. On the other hand, 3D hierarchical structured TiO_2 obviously presented extra small micropores and more mesopores. The micropores in the TiO_2 nanospheres were smaller, signifying that primary particles inside the 3D hierarchical structured TiO_2 were more unified than those in TiO_2 nanospheres. Also, the presence of such mesopores enhanced the perovskite infiltration and improved electron diffusion.[8,36] The side-view SEM pictures of the corresponding ETLs are displayed in Fig. 2c and

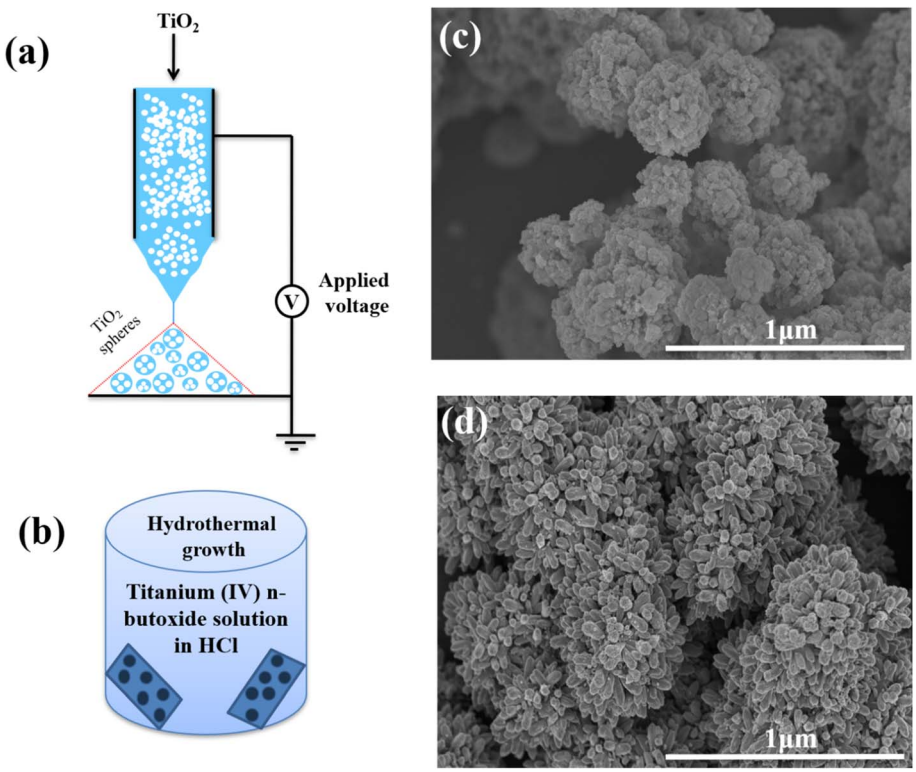

Fig. 1 Schematic of (a) TiO_2 nanospheres deposited *via* an electrospray technique, (b) TiO_2 3D hierarchical structure formed *via* a hydrothermal process, and SEM images of (c) TiO_2 nanospheres and (d) TiO_2 3D hierarchical structure.

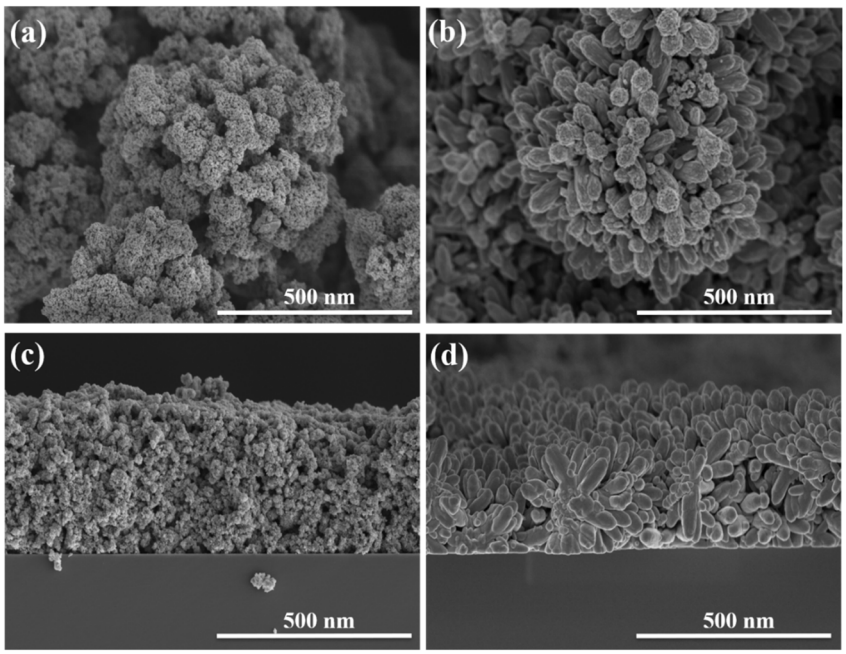

Fig. 2 High resolution SEM images of (a) TiO_2 nanospheres and (b) TiO_2 3D hierarchical structure. Side-view SEM images of (c) TiO_2 nanospheres and (d) TiO_2 3D hierarchical structure.

d, respectively. It can be clearly seen that both types of novel nanostructures entirely cover the entire cross-section of glass substrate. The crystallinity and phase confirmation of the synthesized TiO_2 nanospheres was performed using XRD patterns (Fig. S1†). The diffraction peaks for TiO_2 nanospheres represented the anatase phase of TiO_2 (JCPDS 21-1272). The purity of TiO_2 spheres was confirmed since there were no peaks related with brookite or rutile phases.[8]

To evaluate the performance of TiO_2 nanostructures in perovskite devices, cells assembled with FTO/TiO_2-nanostructured ETL/$MAPbI_3$/spiro-OMeTAD/Au were fabricated. The *J–V* curves of the PSCs made with TiO_2-nanostructured ETLs both in the forward and reverse sweeps are shown in Fig. 3a. The values of the photovoltaic parameters, such as open-circuit voltage (V_{OC}), power conversion efficiency (PCE), fill factor (FF) and short-circuit-current density (J_{SC}), of the related cells are listed in Table 1. PSCs constructed using TiO_2 nanosphere ETLs presented average PCE of 16.10%, with a J_{SC} of 21.3 mA cm^{-2}, V_{OC} of 1050 mV, and an FF of 72%. Meanwhile, devices made with a TiO_2 3D hierarchical structure over nanospheres, verified the improved device performance (average PCE of 19.54%) with no hysteresis. The enhanced performance of the TiO_2 3D hierarchical structure-based devices is attributed to the greater electron transport features and efficient $CH_3NH_3PbI_3$ infiltration inside the minute inner pores as shown in one of our previous works using a side-view SEM image of a whole perovskite device.[36]

In response to solar light irradiation, photoexcited electrons can be produced in the perovskite absorber. The electrons are then inserted into the conduction band (CB) of TiO_2 and propagated over the TiO_2 film in the direction of FTO. A fragment of the inserted electrons might be vanished owing to the electron–hole recombination in the valence band (VB) of the perovskite absorber or the highest occupied molecular orbital (HOMO) of the hole transporting layer.[40] We trust that this type of charge inoculation and conveyance developments are delicately influenced by morphology of the TiO_2 layer. In order to examine the effect of TiO_2 morphology on the kinetics of charge inoculation and conveyance and the photovoltaic performance of perovskite devices, two different kinds of time-determined spectroscopic approaches were utilized as shown in Fig. 4. Initially, to assess the competence of charge inoculation from perovskite to TiO_2, we performed the steady-state PL of PSC devices (Fig. 4a). The PL intensity from TiO_2 3D hierarchical structure-based devices declined, which was either due to (1) radiative or nonradiative deterioration of photoexcited electrons back to the bottom level of the perovskite absorber or (2) electron inoculation through perovskite to TiO_2. The faster decline in PL peak intensity suggested that the electron inoculation from perovskite to TiO_2 became more rapid owing to the increase in roughness factor of the TiO_2 layer.[40] These findings clearly proved that the TiO_2 layer composed of a 3D hierarchical structure is extremely beneficial compared with TiO_2 nanospheres to attain effective electron inoculation from perovskite to TiO_2. Furthermore, we obtained the electron lifetime of photo-inoculated electrons in the TiO_2 film *via* intensity-modulated photovoltage spectroscopy (IMVS),[36] as revealed in Fig. 4b. The values of time constant signified that the lifetime of photoinduced electrons lasted as a result of the charge reunion among the CB of the TiO_2 layer and the VB of perovskite or the HOMO of the hole transporting layer.[40–42] It can be clearly observed that lifetime significantly differs depending on the category of TiO_2 morphology utilized in the perovskite devices (Fig. 4b).

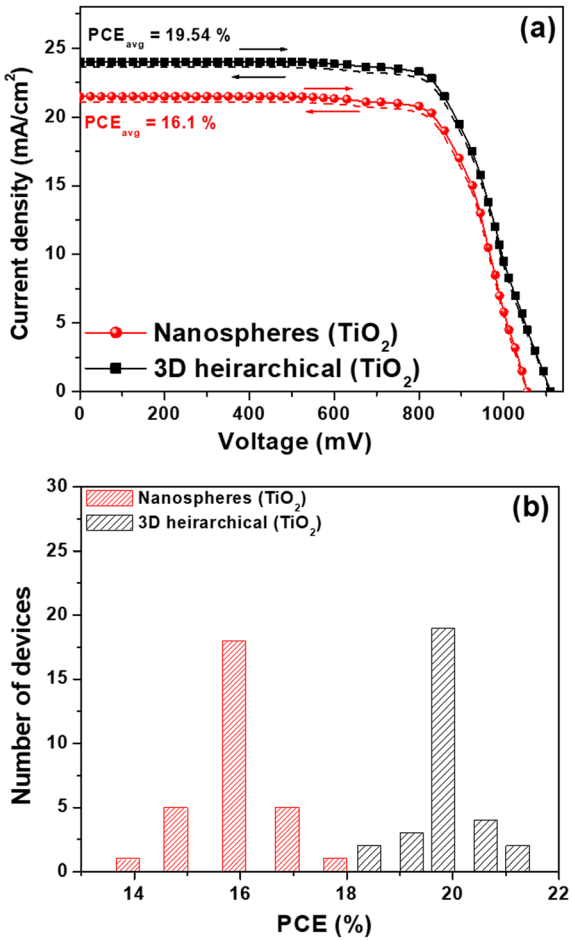

Fig. 3 Assessment of (a) *J–V* plots of TiO_2 nanospheres and TiO_2 3D hierarchical structure, and (b) bar graphs of the matching cells showing the differences in efficiency for 30 separate cells.

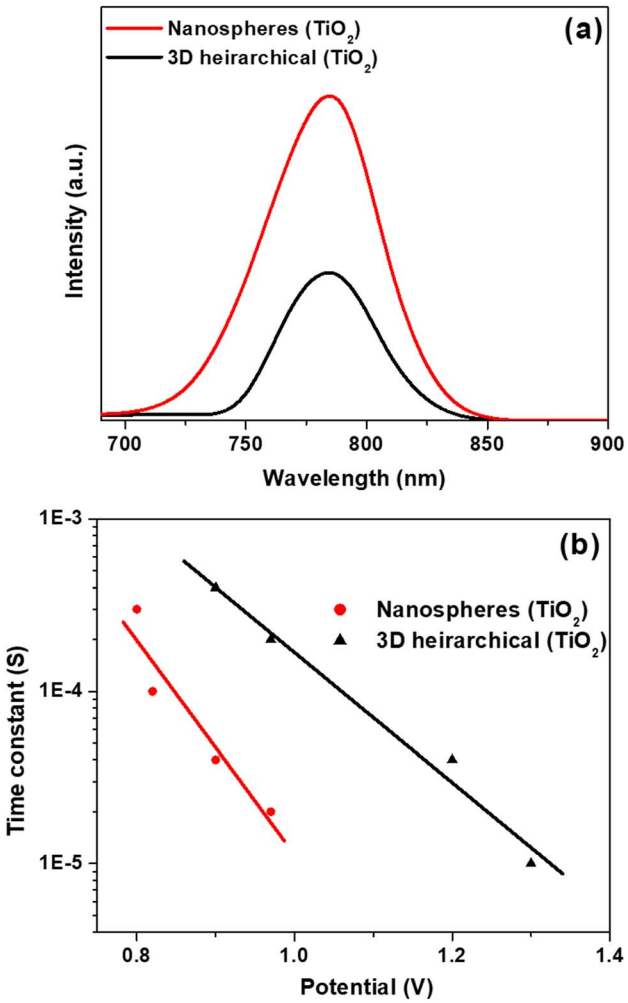

Fig. 4 (a) Steady-state PL spectra of perovskite absorber film coated on TiO_2 nanostructures, and (b) electron lifetime for the corresponding nanostructures.

The plot of EQE *versus* wavelength for typical TiO_2 nanospheres and TiO_2 3D hierarchical structure-based devices (Fig. S2†) shows that TiO_2 3D hierarchical structure-based devices have higher values over the whole spectrum.[8] The cells duplicability was further proven with the help of statistical dispersion of the cells data. Fig. 3b displays the bar chart of efficiency data for 30 separate cells of the corresponding cells. The cells display excellent duplicability in terms of efficiency data for different devices. The average PCE of cells made with the TiO_2 3D hierarchical structure over nanospheres and only TiO_2 nanosphere ETLs are 19.54% and 16.10%, respectively.

The ETL thickness has a vital role in determining the photovoltaic performance, and it is actively tuned *via* experimental settings (namely, spraying time) in the current study. The characteristic *J–V* plots of devices using two different TiO_2-nanostructured ETLs with variable widths are revealed in Fig. S3.† The devices attained the highest efficiency at an optimized ETL thickness of ~810 nm (neither very thin nor very thick). Further increase or decrease in ETL thickness (Fig. S3†) decreased the device efficiency due to incomplete perovskite infiltration into the micropores of ETLs and sluggish electron transport in thicker layers.[40]

We also displayed the steady-state PL spectra (Fig. 4a) of perovskites constructed on two different nanostructures to

Table 1 Device variables attained during various scanning sweeps for two different TiO_2-nanostructured ETLs

ETL	Scan direction	J_{SC} (mA cm^{-2})	V_{OC} (mV)	FF (%)	PCE$_{avg}$ (%)
TiO_2 nanospheres	Reverse	21.5	1050	72	16.25 ± 0.10
	Forward	21.1	1050	72	15.95 ± 0.10
	Average	21.3	1050	72	16.10 ± 0.10
3D hierarchical TiO_2	Reverse	24.0	1110	74	19.71 ± 0.12
	Forward	23.6	1110	74	19.38 ± 0.11
	Average	23.8	1110	74	19.54 ± 0.12

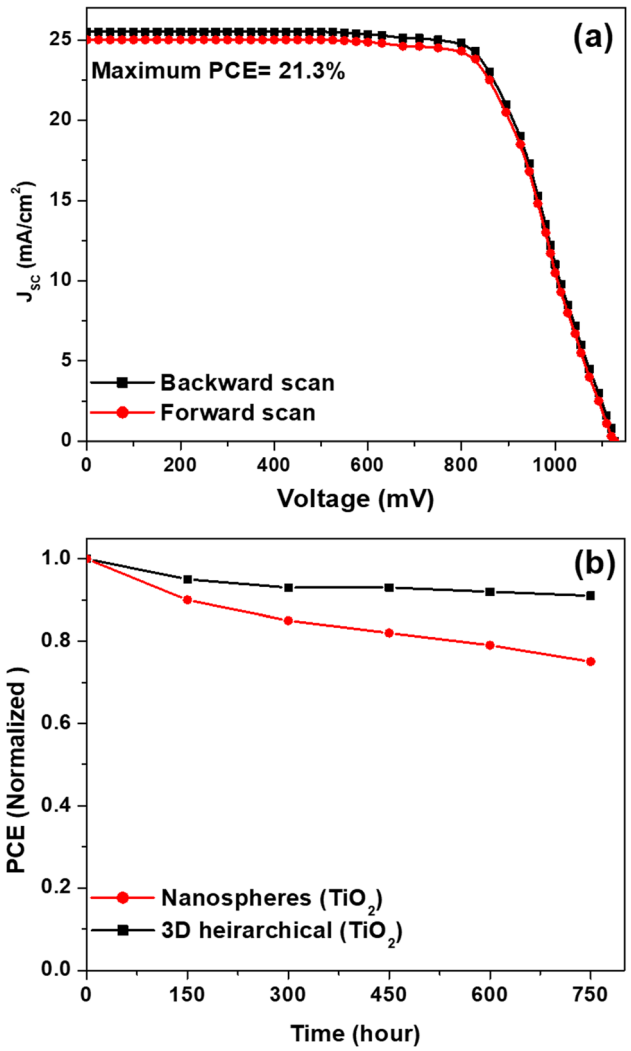

Fig. 5 (a) *J–V* curves (in reverse and forward scans) of the best-performing cell based on TiO_2 3D hierarchical structure and (b) long-term stability test for cells made with TiO_2 nanospheres and TiO_2 3D hierarchical structures.

investigate the reason behind the rapid charge extraction abilities of 3D hierarchical TiO_2-nanostructured ETL compared with the TiO_2 nanospheres. The cells fabricated using 3D hierarchical TiO_2 nanostructures reveal the weak PL peak intensity compared with TiO_2 nanospheres, which improves the electron transfer from perovskites to ETLs.[36,40] Furthermore, an IMVS experiment was investigated (Fig. 4b) to determine the electron lifetime of perovskites coated on two distinct TiO_2 nanostructures. The extended electron lifetime was observed for perovskites made with 3D hierarchical TiO_2 nanostructures rather than TiO_2 nanospheres, signifying the reduced charge recombination.[36,40]

Fig. 5a displays the *J–V* plot and the corresponding performance parameters of the best operating cells made with a TiO_2 3D hierarchical structure over nanospheres, showing a superior J_{SC} of 25.25 mA cm^{-2}, an FF of 75% and a V_{OC} of 1125 mV, offering an average PCE of 21.3% for TiO_2 3D hierarchical structure over nanosphere ETL-based PSCs. The EQE spectrum of the finest operating PSCs fabricated with TiO_2 3D hierarchical structure is shown in Fig. S4.† The obtained J_{SC} value of 25.1 mA cm^{-2} using *J–V* curves (Fig. 5a) matched well with the integrated J_{SC} value of 24.5 mA cm^{-2}. Furthermore, cell stability is vital for the commercialization of devices. Thus, long-term stability assessment was also conducted for the synthesized ETLs, which were stored in ambient environments without any encapsulation (Fig. 5b). The cells made with TiO_2 3D hierarchical structure over nanosphere ETLs revealed consistent performance (maintained over 96% of its initial efficiency value just after preservation for more than 700 h) compared with cells constructed with TiO_2 nanosphere ETLs. This can be attributed to the better resistance of TiO_2 against oxygen and moisture surroundings and better porosity of TiO_2 3D hierarchical structure over nanospheres.

4. Conclusion

Efficient and stable perovskite devices were fabricated with the ETLs composed of a TiO_2 3D hierarchical structure over nanospheres. A facile and low temperature synthesis scheme was suggested for the fabrication of these ETLs. These films not only offered extended surface area and porosity but also rapid charge inoculation and conveyance, which were essential for realizing high performance perovskite devices. Devices made with TiO_2 3D hierarchical structure over nanospheres provided a high PCE of 21.3%, which is the highest PCE ever gained using hierarchical TiO_2 photoelectrodes. These results clearly show that 3D hierarchical TiO_2 nanostructures have enormous roles in building next generation mesostructured photovoltaics. Moreover, these ETLs are expected to offer excellent application potential in diverse fields.

Data availability

Data for this study are available from the authors upon request.

Conflicts of interest

The authors have no competing interests to declare that are relevant to the content of this article.

Acknowledgements

This work was supported by the Higher Education Commission (HEC), Pakistan.

References

1 K. Mahmood, S. Sarwar and M. T. Mehran, *RSC Adv.*, 2017, **7**, 17044–17062.
2 J. Yan and B. R. Saunders, *RSC Adv.*, 2014, **4**, 43286–43314.
3 G. E. Eperon, S. D. Stranks, C. Menelaou, M. B. Johnston, L. M. Herz and H. J. Snaith, *Energy Environ. Sci.*, 2014, **7**, 982–988.

4 R. Sharif, A. Khalid, S. W. Ahmad, A. Rehman, H. G. Qutab, H. H. Akhtar, K. Mahmood, S. Afzal and F. Saleem, *Nanoscale Adv.*, 2023, **5**, 3803–3833.
5 K. Mahmood, A. Khalid and M. T. Mehran, *Sol. Energy*, 2018, **173**, 496–503.
6 W. Tress, N. Marinova, T. Moehl, S. M. Zakeeruddin, M. K. Nazeeruddin and M. Grätzel, *Energy Environ. Sci.*, 2015, **8**, 995–1004.
7 H. Tsai, W. Nie, J. C. Blancon, C. C. Stoumpos, R. Asadpour, B. Harutyunyan, A. J. Neukirch, R. Verduzco, J. J. Crochet and S. Tretiak, *Nature*, 2016, **536**, 312–316.
8 K. Mahmood, B. S. Swain and A. Amassian, *Adv. Mater.*, 2015, **27**, 2859–2865.
9 I. S. Yang, J. S. You, S. Do Sung, C. W. Chung, J. Kim and W. I. Lee, *Nano Energy*, 2016, **20**, 272–282.
10 Y. Zhou and M. Antonietti, *J. Am. Chem. Soc.*, 2003, **25**, 14960–14961.
11 P. Luo, H. Niu, G. Zheng, X. Bai, M. Zhang and W. Wang, *Electrochim. Acta*, 2010, **55**, 2697–2705.
12 H. Wang, R. Jiang, M. Sun, X. Yin, Y. Guo, M. He and L. Wang, *J. Mater. Chem. C*, 2019, **7**, 1948–1954.
13 S. Ma, T. Ye, T. Wu, Z. Wang, S. Ramakrishna, C. Vijila and L. Wei, *Sol. Energy Mater. Sol. Cells*, 2019, **191**, 389–398.
14 Y. Zhang, L. Wu, E. Xie, H. Duan, W. Han and J. Zhao, *J. Power Sources*, 2009, **189**, 1256–1263.
15 M. Fujimoto, T. Kato, W. Takashima, K. Kaneto and S. Hayase, *J. Electrochem. Soc.*, 2006, A826–A829.
16 X. Li, Y. Zhang, Z. Zhang, J. Zhou, J. Song, B. Lu, E. Xie and W. Lan, *J. Power Sources*, 2011, **196**, 1629–1644.
17 D. Hwang, H. Lee, S. Y. Jang, S. M. Jo, D. Kim, Y. Seo and D. Y. Kim, *ACS Appl. Mater. Interfaces*, 2011, **7**, 2719–2725.
18 P. Y. Lin, Y. Y. Chen, T. F. Guo, Y. S. Fu, L. C. Lai and C. K. Lee, *RSC Adv.*, 2017, **18**, 10985–10991.
19 W. Q. Wu, H. L. Feng, H. S. Rao, Y. F. Xu, D. B. Kuang and C. Y. Su, *Nat. Commun.*, 2014, **5**, 3968.
20 X. Sheng, D. He, J. Yang, K. Zhu and X. Feng, *Nano Lett.*, 2014, **14**, 1848–1852.
21 S. H. Ahn, D. J. Kim, W. S. Chi and J. H. Kim, *Adv. Mater.*, 2013, **25**, 4893–4897.
22 L. Passoni, F. Ghods, P. Docampo, A. Abrusci, J. Martí-Rujas, M. Ghidelli, G. Divitini, C. Ducati, M. Binda and S. Guarnera, *ACS Nano*, 2013, **7**, 10023–10031.
23 W. Q. Wu, Y. F. Xu, H. S. Rao, C. Y. Su and D. B. Kuang, *J. Am. Chem. Soc.*, 2014, **136**, 6437.
24 I. S. Cho, Z. B. Chen, A. J. Forman, D. R. Kim, P. M. Rao, T. F. Jaramillo and X. L. Zheng, *Nano Lett.*, 2011, **11**, 4978.
25 D. H. Lee, Y. Rho, F. I. Allen, A. M. Minor, S. H. Ko and C. P. Grigoropoulos, *Nanoscale*, 2013, **5**, 11147.
26 J. W. Shiu, C. M. Lan, Y. C. Chang, H. P. Wu, W. K. Huang and E. W. G. Diau, *ACS Nano*, 2012, **6**, 10862.
27 S. N. Habisreutinger, L. Schmidt-Mende and J. K. Stolarczyk, *Angew. Chem., Int. Ed.*, 2013, **52**, 7372.
28 N. Cai, S. J. Moon, L. Cevey-Ha, T. Moehl, R. Humphry-Baker, P. Wang, S. M. Zakeeruddin and M. Grätzel, *Nano Lett.*, 2011, **11**, 1452.
29 Z. Fang, G. Wang, C. Guan, J. Zhang and Q. Xiang, *Angew. Chem., Int. Ed.*, 2024, **63**, e202411219.
30 C. Guan, Y. Liao and Q. Xiang, *Sci. China Mater.*, 2024, **67**, 473–483.
31 S. Javed, M. A. Akram and M. Mujahid, *CrystEngComm*, 2014, **48**, 10937.
32 J. Shi, Y. Hara, C. L. Sun, M. A. Anderson and X. D. Wang, *Nano Lett.*, 2011, **11**, 3413.
33 D. Li and Y. Xia, *Nano Lett.*, 2003, **3**, 555.
34 W. Q. Wu, H. S. Rao, Y. F. Xu, Y. F. Wang, C. Y. Su and D. B. Kuang, *Sci. Rep.*, 2013, **3**, 1892.
35 K. Mahmood, M. Alzaid, A. Khalid, R. A. Malik, H. G. Qutab, S. W. Ahmad, A. Maqbool, F. Alsalh and N. Almoisheer, *Surf. Coat. Technol.*, 2021, **416**, 127160.
36 M. Hameed, K. Mahmood, M. Imran, F. Nawaz and M. T. Mehran, *Nanoscale Adv.*, 2019, **1**, 1297–1304.
37 K. Mahmood, A. Khalid, M. Hameed, F. Rehman, M. T. Mehran and R.-H. Song, *Appl. Phys. A*, 2018, **124**, 1–6.
38 K. Mahmood and A. Khalid, *Mater. Lett.*, 2018, **224**, 78–81.
39 D. Hwang, H. Lee, S.-Y. Jang, S. M. Jo, D. Kim, Y. Seo and D. Y. Kim, *ACS Appl. Mater. Interfaces*, 2011, **3**, 2719–2725.
40 I. S. Yang, J. S. You, S. D. Sung, C. W. Chung, J. Kim and W. I. Lee, *Nano Energy*, 2016, **20**(20), 272–282.
41 J. van de Legemaat and A. J. Frank, *J. Phys. Chem.*, 2001, **B105**, 11194–11205.
42 K. D. Benkstein, N. Kopidakis, J. van de Legemaat and A. J. Frank, *J. Phys. Chem. B*, 2003, **107**, 7759–7767.